Received: 20 February 2020 | Revised: 25 May 2020 | Accepted: 31 May 2020

DOI: 10.1002/bit.27446

ARTICLE

BIOTECHNOLOGY AND BIOENGINEERING WILEY

Engineering slit-like channels for studying the growth of epithelial tissues in 3D-confined spaces

Laura Alaimo | Marine Luciano | Danahe Mohammed | Marie Versaevel | Céline Bruyère | Eléonore Vercruysse | Sylvain Gabriele

University of Mons, Laboratory for Complex Fluids and Interfaces, Mechanobiology and Soft Matter Group, CIRMAP, Research Institute for Biosciences, Place du Parc, Mons, Belgium

Correspondence
Sylvain Gabriele, University of Mons, Laboratory for Complex Fluids and Interfaces, Mechanobiology and Soft Matter Group, CIRMAP, Research Institute for Biosciences, Place du Parc, 20 B-7000 Mons, Belgium.
Email: sylvain.gabriele@umons.ac.be

Funding information
F.R.S.-FNRS, Grant/Award Number: Crédit de Recherches - J009916F

Abstract

The development of epithelial lumens in ducts is essential to the functioning of various organs and in organogenesis. Ductal elongation requires the collective migration of cell cohorts in three-dimensional (3D) confined spaces, while maintaining their epithelial integrity. Epithelial lumens generally adopt circular morphologies, however abnormalities in complex physiological environments can lead to the narrowing of glandular spaces that adopt elongated and slit-like morphologies. Here, we describe a simple method to form epithelial tissues in microchannels of various widths (100–300 μm) with a constant height of 25 μm that mimic elongated geometries of glandular spaces. The significance of this biomimetic platform has been evidenced by studying the migration of epithelial cell sheets inside these narrow slits of varying dimensions. We show that the growth of epithelial tissues in 3D-confined slits leads to a gradient of cell density along the slit axis and that the migration cell velocity depends on the extent of the spatial confinement. Our findings indicate that nuclear orientation is higher for leader cells and depends on the slit width, whereas YAP protein was predominantly localized in the nucleus of leader cells. This method will pave the way to studies aiming at understanding how 3D-confined spaces, which are reminiscent of in vivo pathological conditions, can affect the growth and the homeostasis of epithelial tissues.

KEYWORDS
cell migration, confined environment, epithelial tissues, slit-like microchannels

1 | INTRODUCTION

Epithelial lumens are found in many organs of the human body and generally adopt circular or ellipsoidal morphologies (Hoijman, Rubbini, Colombelli, & Alsina, 2015). These curved epithelial monolayers enclose a central cavity, also named "lumen," which is central to the functioning of many organs and essential in organogenesis (Lubarsky & Krasnow, 2003; Martín-Belmonte et al., 2008; Mohammed, Versaevel, et al., 2019). The tubulogenesis of epithelia is based on the collective migration of epithelial cell cohorts, such as observed in ductal elongation (Huebner & Ewald, 2014; Williams & Daniel, 1983) and is modulated by external physical cues such as confinement and out-of-space curvature (Xi, Sonam, Beng Saw, Ladoux, & Teck Lim, 2017). However, abnormalities in complex physiological environments can lead to the narrowing of glandular spaces that adopt elongated and slit-like morphologies, which are, for instance, reminiscent of the usual duct hyperplasia of the breast (Bishop et al., 2013) and cervical glandular neoplasia (Loureiro & Oliva, 2014). Most of the previous studies on collective cell migration have employed two-dimensional (2D) flat culture substrates (Tlili et al., 2018; Trepat et al., 2009) that lead to the formation of planar epithelia with morphologies fundamentally distant from lumens morphologies. Recent studies used protein microstripes for studying the collective migration of epithelial cells with chemical boundary restrictions (Mohammed, Charras, et al., 2019; Poujade et al., 2007;

Vedula et al., 2012). Other studies have investigated the role of the out-of-plane curvature by studying the collective motion of epithelial cells on the outer surface of cylindrical fibers (Yevick, Duclos, Bonnet, & Silberzan, 2015) and in the inner surface of microtubes (Xi et al., 2017).

However only few prior studies have investigated the growth of epithelial cell sheets in rectangular microchannels with aspect ratios reminiscent to the geometries of slit-like spaces, as observed in duct hyperplasia of the breast (Bishop et al., 2013). To address this issue, we studied the coordinated migration of Martin-Darby canin kidney (MDCK) epithelial cells into slit-like confined spaces. We show that MDCK cells form lumens in 1:4, 1:8, and 1:12 slit aspect ratios with a constant height of 25 μm. The coordinated migration of MDCK cells on the inner surface of these slit-like microchannels leads to a gradient of cell density along the slit axis, whereas the migration cell velocity depends on the extent of the spatial confinement. Our findings indicate that nuclear orientation is higher for leader cells and depends on the slit width, whereas Yes-associated protein (YAP) protein was predominantly localized in the nucleus of leader cells. Altogether, our findings provide novel insights into the growth of epithelial cell sheets under narrow confinement, which is reminiscent of in vivo pathological scenarios.

2 | MATERIALS AND METHODS

2.1 | Cell culture

Epithelial cells from the Madin–Darby canine kidney cell line (MDCK II, Sigma no. 85011435) were cultured in Dubelcco's modified Eagle's medium supplemented with 10% fetal bovine serum (AE Scientific) and 1% antibiotic (Penicillin, Streptomycin; AE Scientific). Cells were incubated at 37°C with 5% of CO_2 and in an environment saturated in humidity. MDCK cells were cultured into the microchannels in static culturing conditions (i.e. in absence of flow) for 4–8 days.

2.2 | Slit-like microchannels

Microchannels of 100-, 200-, and 300-μm wide, with a constant height of 25 μm, were built in polydimethylsiloxane (PDMS, Sylgard 184 Silicone Elastomer Kit; Dow Corning) using a three step process (Versaevel, Grevesse, Riaz, Lantoine, & Gabriele, 2014). The first step consisted to spin-coat fluorodishes (Cellvis) of 30 mm in diameter with PDMS (10:1 ratio of PDMS to curing agent) at 5,000 rpm (Versaevel, Riaz, Grevesse, & Gabriele, 2013). The corresponding PDMS layer of ~25 μm in thickness was then cured for 4 hr at 60°C (Coppée, Gabriele, Jonas, Jestin, & Damman, 2011). A silicon master was fabricated by deep reactive-ion etching from a chromium photomask (Toppan Photomask, Inc.) and its surface was passivated with vapors of fluorosilane (tridecafluoro-1,1,2,2-tetrahydrooctyl-1-trichlorosilane, Gelest) for 30 min. In a second step, PDMS microchannels of 100-, 200-, and 300-μm wide were obtained by molding the silanized silicon master with PDMS, which was then cured for 4 hr at 60°C. After reticulation, the PDMS microchannels were gently peeled of the silicon wafer and a sharpened blunt needle was used to punch holes at the inlet and outlet. PDMS microchannels were washed in an ultrasonic bath (Bandelin Sonorex Digitec) for 15 min with a detergent solution (Decon 90; Decon Laboratories Limited), then with demineralized water and finally with a 70% ethanol solution. In the third step, PDMS microchannels and PDMS-coated fluorodishes (World Precision Instruments Inc.) were irradiated under plasma for 2 min to create silanol groups on both surfaces. Both activated elements were then assembled together and cured 3 hr at 60°C. Before cell seeding, slit-like channels were first sterilized in ethanol, then rinsed with sterile phosphate-buffered saline (PBS) and finally irradiated for 30 min under a germicidal ultraviolet (UV) lamp. Sterile microchannels were afterwards functionalized for 1 hr at room temperature with a sterile stock solution composed of type-I collagen solution at 10 mg/ml (rat tail type-I collage; Corning) and poly-L-lysine at 0.1% (Sigma-Aldrich) and finally rinsed twice with sterile PBS.

2.3 | Sample fixation and immunostaining

MDCK cells were grown inside PDMS microchannels, then fixed and permeabilized in situ by injecting a solution composed of 4% paraformaldehyde (electron microscopy sciences) with 0.1% Triton X-100 (Sigma) in PBS (×1; Capricorn Scientific) for 10 min at room temperature. Microchannels were rinsed with PBS and incubated for 45 min with a blocking solution containing 1% bovine serum albumin (GE Healthcare) in PBS. The actin cytoskeleton was labeled in green using Alexa 488 phalloidin (1:200; Molecular Probes), DNA was stained in blue with 4′,6-diaminido-2-phenylindole di-hydrochloride (DAPI; 1:200; Thermo Fisher Scientific; D1306) and YAP was labeled with an anti-YAP produced in mice (M01, clone 2F12, 1:100; Abnova) and a secondary anti-mouse-tetramethylrhodamine antibody emitting in the red.

2.4 | Microscopy imaging

Epithelial tissues were observed in epifluorescence and confocal mode with a Nikon Eclipse Ti-E motorized inverted microscope (Nikon C1 scanhead; Nikon, Japan) equipped with × 10, × 20, and × 40 lenses (Riaz, Versaevel, Mohammed, Glinel, & Gabriele, 2016). Epifluorescence images were recorded with a Roper QuantEM:512SC EMCCD camera (Photometrics, Tucson, AZ) using NIS Elements. Advanced Research 4.0 software (Nikon; Photometrics). Confocal images were acquired with NIS Elements Advanced Research 4.0 software (Nikon) by using small Z-depth increments between focal sections (0.15 μm).

2.5 | Image analysis

Fiji software and home-made MATLAB codes have been used to analyze epifluorescent and confocal images (Versaevel, Grevesse, & Gabriele, 2012). The MATLAB code allows the automatic detection of

nuclei stained with Hoechst or DAPI to provide morphological information such as the projected area, the orientation, the nuclear aspect ratio and the cell density in each image. The nuclear aspect ratio was obtained from the ratio between the long and the short axis, leading to values ranging from 0 (elongated nucleus) to 1 (circular nucleus). The cell area (A) and the perimeter (P) were determined by delimiting the contour of the cell with ImageJ (Collins, 2007). Both pieces of information were used to estimate the cell shape index (p_0), such as: $p_0 = P/\sqrt{A}$. To determine the nuclear/cytoplasmic YAP ratio, Z stacks were acquired for each channel on immunostained cells. The middle confocal slice was chosen from the images of the nucleus detected in the DAPI channel. On the corresponding slice in the YAP channel, the average fluorescence intensity in the nucleus and just outside the nucleus (cytoplasm) were measured to determine the cytoplasmic/nuclear YAP ratio.

2.6 | Migrating cell velocity

The migrating front velocity was determined from DIC images taken from Day 1 to Day 8. We measured the position of the growing front in the microchannel for the three microchannel widths (100, 200, and 300 μm). In addition, we used CellTracker software to track the *x*,*y* position of the nucleus of each individual cell overtime, to determine the velocity of leader and follower cells. The nuclei of living MDCK tissues were stained with Hoechst 33342 (Thermo Fisher H3570) at a concentration of 200 ng/ml to follow their *x*,*y* position over time.

2.7 | Statistical analysis

Differences in means between groups were evaluated by two-tailed Student's *t* tests performed in Prism 7 (GraphPad). For multiple comparisons, the differences were determined by using an analysis of variance followed by Tukey's post-hoc test with $^{*}p < .05$; $^{**}p < .01$; $^{***}p < .001$; n.s., not significant. Unless otherwise stated, all data are presented as mean ± standard deviation (*SD*).

3 | RESULTS

3.1 | Formation of epithelial cell sheets inside slit-like microchannels

Based on the literature, we estimated the width of slit-like glandular spaces (Figure 1a,b) found in the cervical carcinoma (Yao, 2009), the

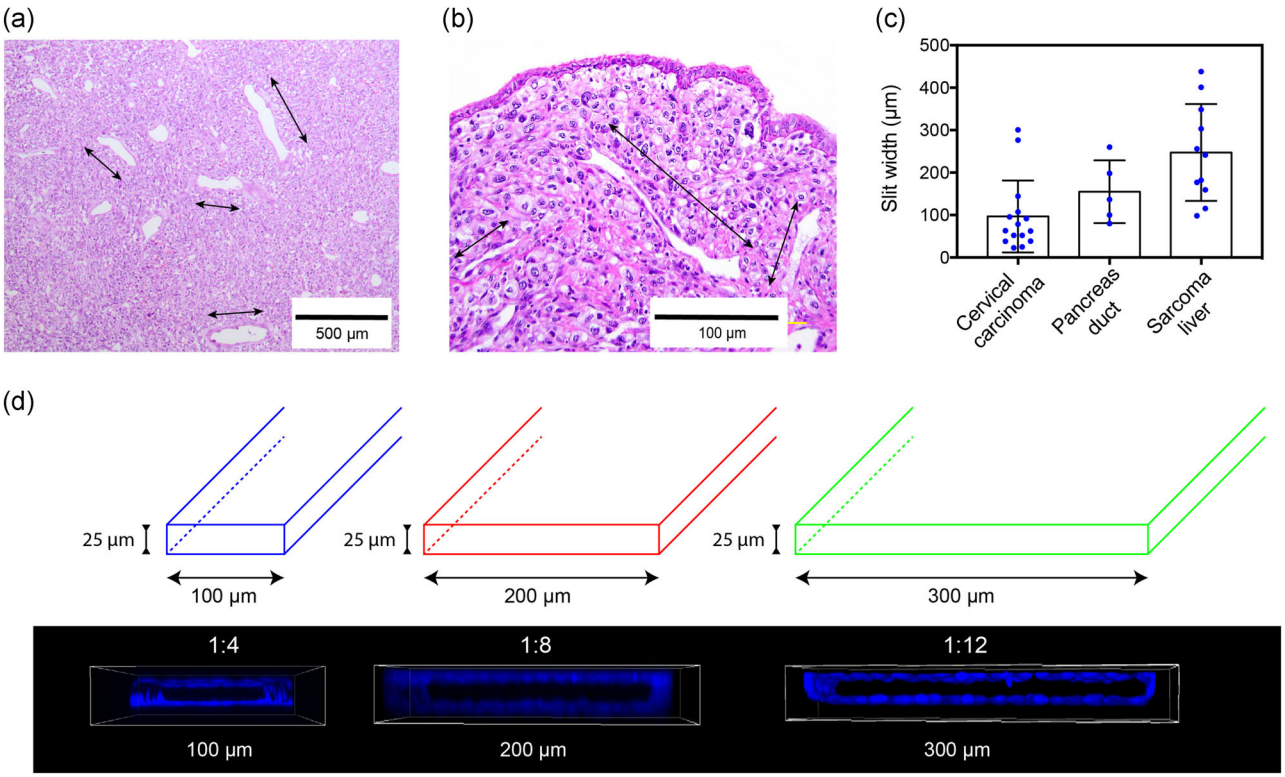

FIGURE 1 Typical examples of slit-like lumens in sections of (a) liver (Janevska et al., 2011) and (b) cervical (Maniar & Wei, 2017) tissues. (c) Width of slit-like capillaries in cervical carcinoma ($n = 15$), pancreas duct ($n = 5$), and sarcoma liver ($n = 11$). Mean ± *SD*. (d) The cross-sectional views of 4',6-diamidino-2-phenylindole (DAPI)-stained nuclei in Martin-Darby canin kidney (MDCK) tissues grown in 1:4 (100-μm wide), 1:8 (200-μm wide) and 1:12 (300-μm wide) rectangular channels demonstrate that epithelial tissues line the interior surface of the slit-like microchannels and form hollow lumens, as observed in vivo [Color figure can be viewed at wileyonlinelibrary.com]

pancreas intralobular duct (Carpino et al., 2016) and the sarcoma livers (Janevska et al., 2011). As shown in Figure 1c, we found mean slit widths of 96.7 ± 84.7, 155 ± 74, and 247.3 ± 114 μm for the cervical carcinoma, the pancreas intralobular duct and the sarcoma livers, respectively. We developed therefore rectangular microchannels of various widths (100, 200, and 300 μm) with a constant height of 25 μm. These different aspect ratios (1:4, 1:8, and 1:12) allow to mimic the dimensions of slit-like glandular spaces encountered in different organs (Figure 1d). Microchannels were made in a polydimethylsiloxane (PDMS) elastomer of 3 MPa in Young's modulus, which is optically transparent, gas permeable and biocompatible. To allow the formation of specific cell-substrate adhesions, the inner surface of the PDMS microchannels (Figure S1) was incubated over 1 hour with a solution of collagen type-I (250 μg/ml) and poly-L-lysine (35 μg/ml). Madin–Darby canine kidney cells (MDCK II) were gently seeded at the inlet of the microchannel and then grown inside the microchannels in static culturing conditions (i.e. in absence of flow) for 2–8 days in culture medium at 37°C and 5% of CO_2. As shown in Figure 1d, the cross-sectional views of DAPI-stained nuclei in MDCK tissues grown in 1:4 (100-μm wide), 1:8 (200-μm wide) and 1:12 (300-μm wide) rectangular channels demonstrate that epithelial tissues line the interior surface of the slit-like microchannels (Supporting Information Movie 1) and form hollow lumens (Supporting Information Movie 2). Morphologies and dimensions of the epithelial lumen formed in the microchannels are reminiscent of intercalated ducts that form part of the intralobular duct (Janevska et al., 2011) in both the pancreas and in salivary glands (de Paula et al., 2017; Gittes, 2009; Reichert & Rustgi, 2011).

3.2 | Cell density varies along the microchannels

As shown in Figure 2a, we defined three successive zones of interest of 300-μm long each. The location of the rear zone was fixed and close to the inlet where cells were injected at the beginning of the experiment. The front zone of 300-μm long started from the growing extremity of the epithelial tissue towards the rear of the tissue. Due to the growth of the tissue, the spatial location of the front zone was ever more distant with time from the rear. The intermediate (or interm) zone of 300-μm long was located at the center between the rear and front zones (Figure S2). After 4 days in culture in static culturing conditions (i.e. in absence of flow), epithelial tissues were immunostained with DAPI (DNA) and AlexaFluor 488 phalloidin (actin filaments). The three zones were imaged by confocal microscopy to determine the main morphological parameters of epithelial tissues grown into 100, 200, and 300 μm slit-like microchannels (Figure 2a). As shown in Figure 2b, we observed an abrupt decrease of the cell density from the rear to the front of the slit-like

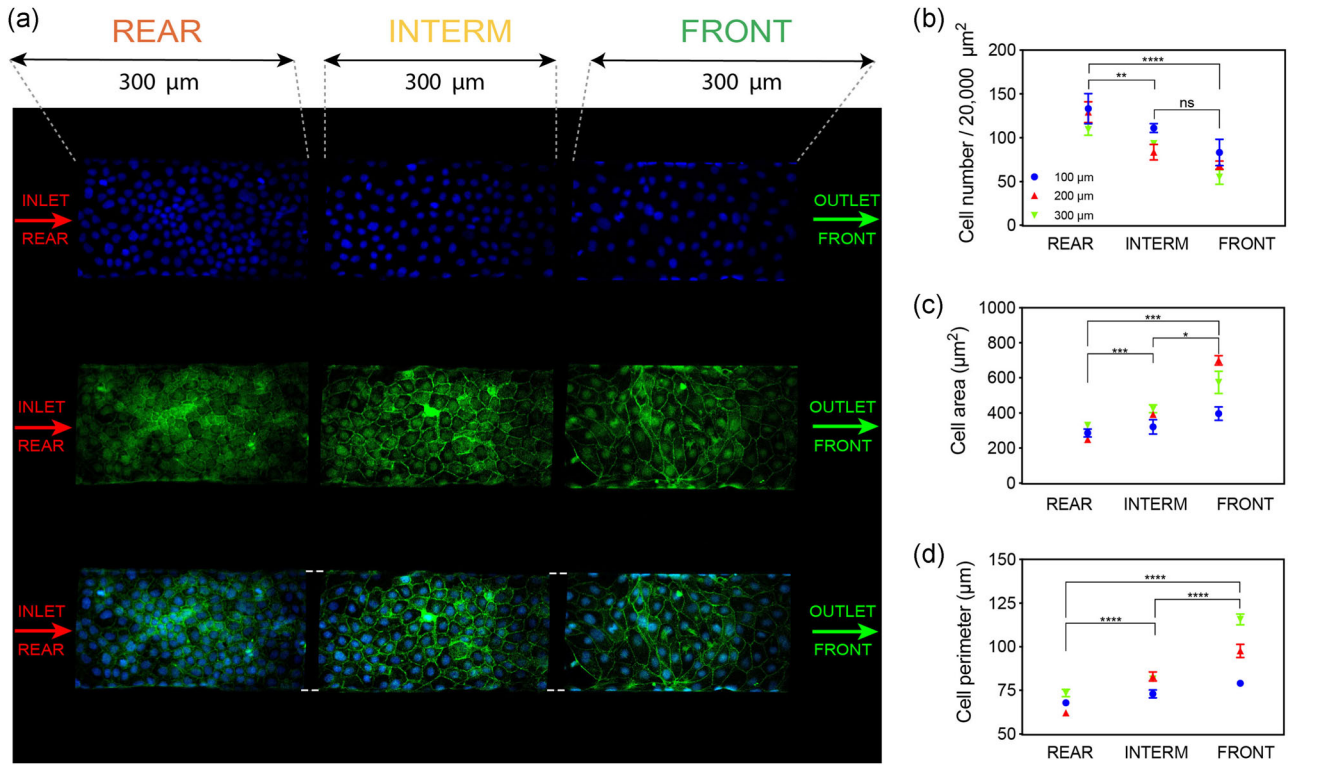

FIGURE 2 (a) Typical example of the three successive zones: rear, intermediate, and front of an epithelial tissue grown in a 200-μm-wide slit-like microchannel. Each zone is 300-μm long. Nuclei are stained in blue with 4',6-diamidino-2-phenylindole (DAPI) and actin filaments are stained in green with AlexaFluor 488. (b) Cell density, (c) cell area, and (d) cell perimeter for rear, interm, and front zones in 100-, 200-, and 300-μm-wide slit-like channels. Mean ± *SD* for 11–13 replicates with $50 \le n \le 245$ by replicate. *$p < .05$, **$p < .01$, ***$p < .001$, ****$p < .0001$ and n.s. not significant [Color figure can be viewed at wileyonlinelibrary.com]

microchannels, regardless of their aspect ratios. We found that both cell area (Figure 2c) and perimeter (Figure 2d) increased from the rear to the front of the microchannels, whereas larger cells were found at the front of the 300-μm-wide microchannel. The evolution of the cell perimeter indicated that follower cells at the rear are characterized by less cell-cell interactions than leaders cells located at the growing front. Taken together, these findings indicate that epithelial cell sheets grown in confined slit-like microchannels were characterized by a gradient of cell density along the channel axis, defining large leader cells at the front and compacted followers at the rear, which was observed recently to modulate the migration speed of epithelial tissues (Mohammed, Charras, et al., 2019).

3.3 | Ageing leads to the fluidization of the front

Considering the evolution of both the cell area and the cell perimeter, we determined the cell shape index (p_0), as introduced by Bi, Lopez, Schwarz, and Manning (2015) to describe the jamming state of epithelial tissues (Trepat et al., 2009). As shown in Figure 3a, the shape index was defined by the ratio between the cell perimeter and the square root of the cell area and describes the jamming transition ($p_0 = 3.81$) of epithelial tissues from a "solid" to a "fluid" state. Indeed, previous studies have shown that epithelial tissues can undergo a critical transition from solid to fluid at $p_0 = 3.81$ (Angelini et al., 2011; Farhadifar, Röper, Aigouy, Eaton, & Jülicher, 2007; Kim & Hilgenfeldt, 2015; Szabó et al., 2006; Vicsek & Zafeiris, 2012). Epithelial tissues behave as a rigid solid when $p_0 < 3.81$ and there are finite energetic barriers for a cell to move or rearrange, whereas tissues behave as a fluid with a vanishing shear modulus for $p_0 > 3.81$. We then considered the evolution of the cell shape index (p_0) for the rear and the front of epithelial tissues at Day 4 in 100-, 200-, and 300-μm-wide microchannels. As shown in Figure 3b, there was no statistical difference of the cell shape index between the rear and front zones for the whole range of microchannel widths, except for the rear part of the 200-μm-wide microchannel. Indeed, both zones exhibited p0 values above the solid to fluid transition ($p_0 = 3.81$), suggesting that the rear and front zones at Day 4 behaved as a fluid, regardless of the channel size. Interestingly, even if we observed large variations of cell densities between rear and front zones, these did not affect the jamming state of the tissues, suggesting that cell density is not a key determinant of jamming within epithelium tissues. To gain further insight into this mechanism, we quantified the cell shape index of mature tissues at Day 6 and Day 8. Surprisingly, our findings showed that the more the front of the tissue was aged, the more the cell shape index p_0 increased (Figure 3c), whereas the rear part of matured epithelial tissues exhibited a constant value of p_0 from Day 4 to Day 8, regardless of the slit width (Figure 3d). Our findings suggest that the maturation of epithelial tissues in 3D-confined microchannels leads to a fluidization of their growing front, which may be explained by a maturation of cell-cell contacts at the leading front (Garcia et al., 2015).

We next investigated whether a fluidization of the advancing front in matured tissues affects the migration velocity. To answer this question, we performed time-lapse experiments at days 1 (young tissues) and 6 (aged tissues) on epithelial cell sheets growing in microchannels of 100, 200 and 300 μm to determine the migrating cell velocity of the front edge (Figure 4a,b). We observed a significant increase of the front velocity at Day 1 as a function of the microchannel width. Indeed, our results showed a mean migration velocity of 0.14 ± 0.04 μm/min for 100-μm-wide microchannels and 0.27 ± 0.03 μm/min for 300-μm-wide microchannels (Figure 4c). The wider the slit-like microchannel, the larger is the migrating cell velocity for young tissues. Interestingly, the migrating cell velocity of aged tissues (Day 6) followed a similar behavior but exhibited velocities three times slower than young tissues. Taken together, these results suggest that the widening of slit-like microchannels allows to increase the migrating cell velocity of epithelial tissues, whereas ageing leads to a higher fluidization of the front edge and slower migrating cell velocities.

3.4 | YAP protein was predominantly localized in the nucleus of leader cells

The next question we addressed was whether variations of the spatial confinement imposed by the geometry of slit-like microchannels could affect mechanotransduction pathways (Mohammed, Versaevel, et al., 2019). Recent studies have suggested that Yes-associated protein (YAP), a central transcriptional regulator implicated in controlling organ body and size, promotes both cell migration and barrier function of epithelial tissues maintenance by increasing the turnover of cadherin (Neto et al., 2018). In addition, accumulating evidence suggests that the activation of YAP proteins can be regulated by physical constraints of the cell microenvironment (Dupont et al., 2011; Furukawa, Yamashita, Sakurai, & Ohno, 2017; Mohammed, Versaevel, et al., 2019). However it is not known whether YAP expression and activity can be modulated during the growth of epithelial tissues in confined spaces.

As shown in Figure 5a, the alignment of the long nuclear axis with the microchannel axis increased from the rear to the front. We found that larger the microchannel, the higher the nuclear orientation (Figure 5a). In addition, we found that the nuclear aspect ratio increased slightly from the rear to the front (Figure 5b), suggesting that the nuclei of leader cells were more rounded than those of followers. Interestingly, our findings indicate that the cellular area scaled linearly with the nuclear area (Figure 5c). This observation demonstrates that the nuclei adapted their morphology to the variations of cellular areas, regardless of their position in the tissue. As shown for 200-μm-wide microchannels in Figure 5d, we then measured the ratio of fluorescence intensity between cytoplasmic and nuclear YAP. We observed a decrease of the cytoplasmic to nuclear YAP ratio from the rear to the front, regardless the microchannel width (Figure 5e–g). Our findings indicated that YAP was significantly

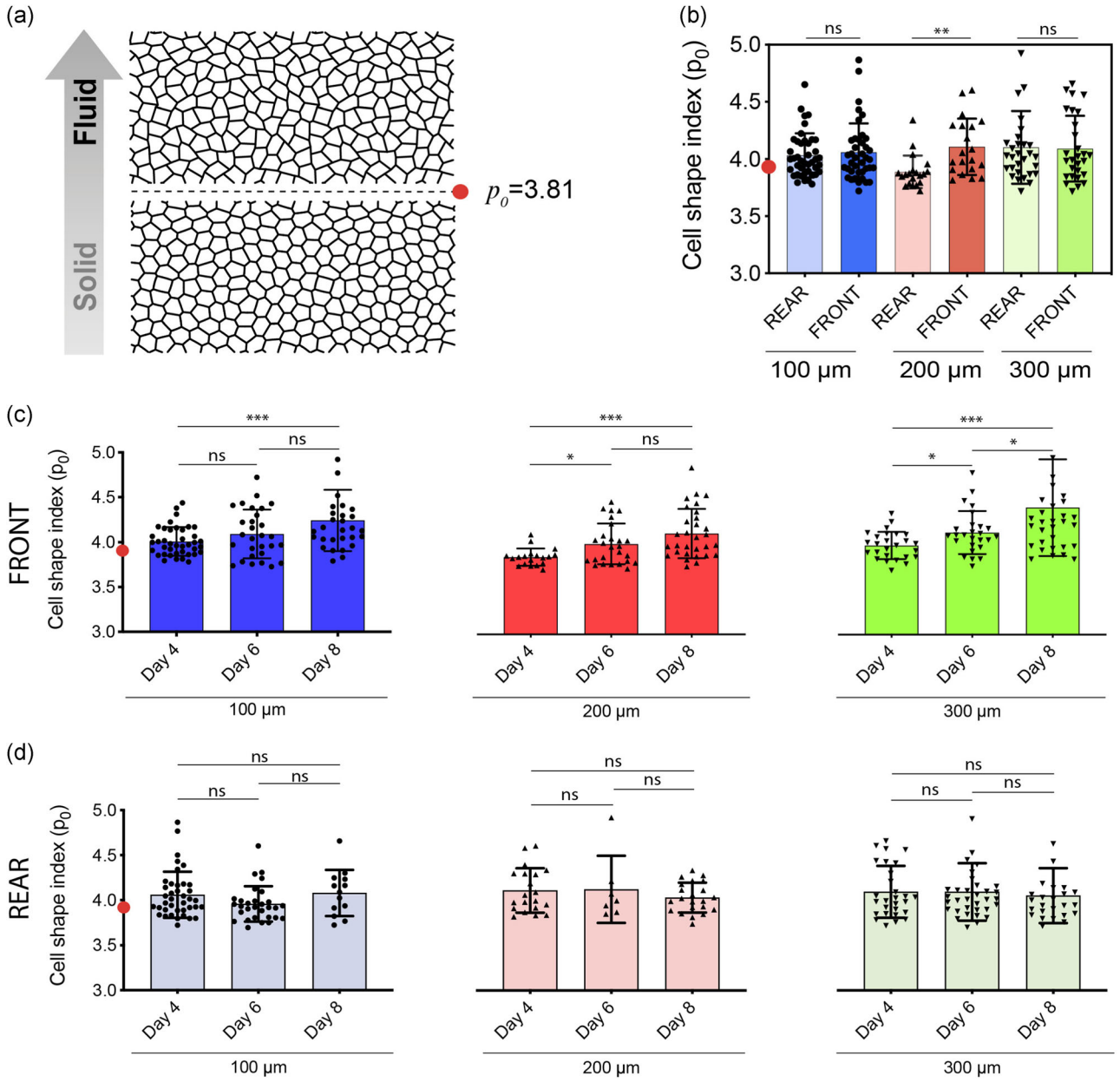

FIGURE 3 (a) Schematic representation of the jamming transition ($p_0 = 3.81$) in epithelial tissues from a solid-like to a fluid-like behavior. (b) Evolution of the cell shape index (p_0) at Day 4 for rear and front zones in 100 µm (blue), 200 µm (red), and 300 µm (green) slit-like microchannels. Evolution of the cell shape index (p_0) of the (c) rear and (d) front zones in 100 µm (blue), 200 µm (red) and 300 µm (green) slit-like microchannels at Days 4, 6 and 8. The red dot corresponds to $p_0 = 3.81$. Mean ± *SD* with $11 \leq n \leq 31$ for each condition. $^*p < .05$, $^{**}p < .01$, $^{***}p < .001$ and n.s. not significant [Color figure can be viewed at wileyonlinelibrary.com]

accumulated in the nucleus of leader cells and therefore activated. Our results are in agreement with recent reports indicating that YAP localized almost exclusively to the nucleus in MDCK tissues with a low cell density, whereas YAP was distributed to both cytoplasm and nucleus at high cell density. (Bruyère et al., 2019). To confirm that the variations of YAP localization observed in the different zones of confined epithelial tissues were related to changes in cell density, we performed additional measurements of YAP localization on flat unconfined MDCK tissues with high (1.2×10^6 cells/cm^2) and low (4×10^5 cells/cm^2) cell densities (Figure S3).

4 | DISCUSSION

The collective migration of epithelial cells in a confined microenvironment is required to form various epithelial luminal architectures, which are essential to the functioning of the organs and for organogenesis. To this aim, epithelial cells need to migrate collectively in complex microenvironments, while maintaining the epithelial integrity. However, conventional assays using flat culture substrates fail to replicate confined microenvironments encountered by epithelial cells. To address this issue, we describe here a simple method

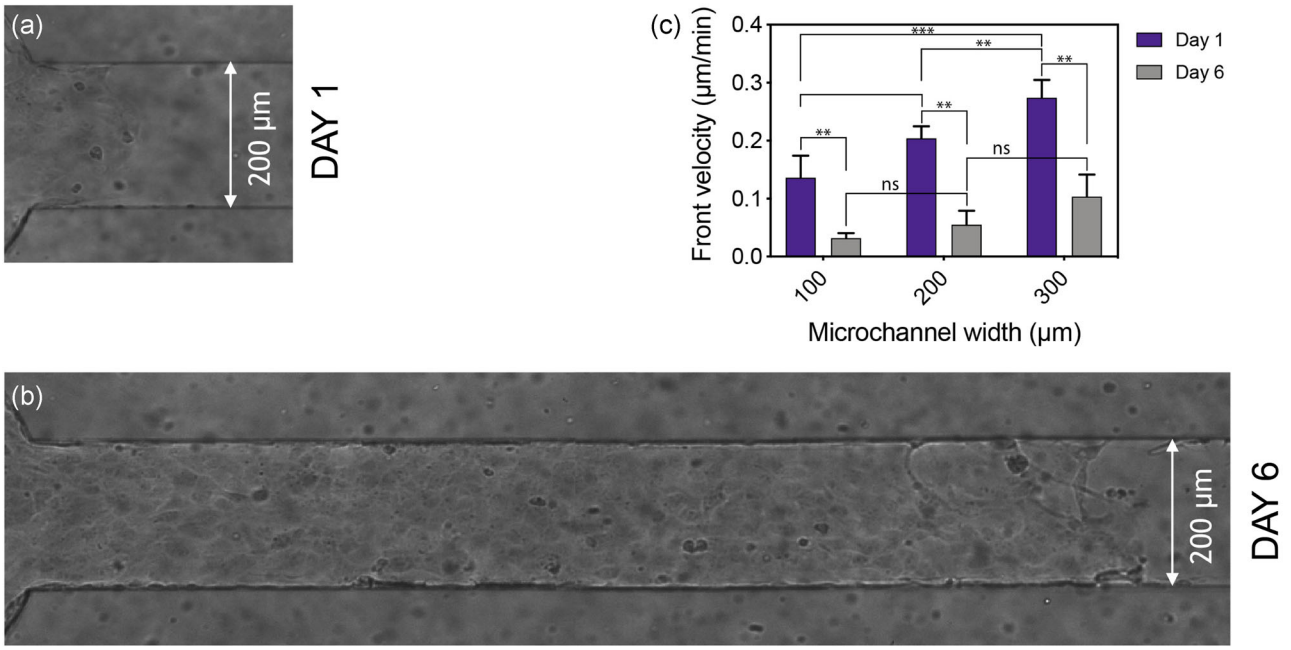

FIGURE 4 Typical differential interference contrast (DIC) image of an epithelial tissue grown in a 200-µm-wide slit-like microchannel at (a) Day 1 and (b) Day 6. (c) Front velocity in 100-, 200-, and 300-µm-wide slit-like microchannels at Day 1 (in purple) and Day 6 (in gray). Mean ± *SD* with $8 \le n \le 14$ for each condition. $^{**}p < .01$, $^{***}p < .001$ and n.s. not significant [Color figure can be viewed at wileyonlinelibrary.com]

to form epithelial tissues in microchannels of various widths (100–300 µm) with a constant height of 25 µm, that mimic elongated geometries of glandular spaces. We validated this platform by studying the coordinated migration of Madin–Darby Canin Kidney (MDCK) epithelial cells into slit-like microchannels of 100-, 200-, and 300-µm wide with a constant height of 25 µm.

We demonstrated that epithelial cells line the interior surfaces of the microchannels and collectively migrated within the slit-like spaces, while maintaining tissue cohesion. We observed the formation of a lumen in slit-like microchannels of 1:4 (100-µm wide), 1:8 (200-µm wide) and 1:12 (300-µm wide) aspect ratios, as observed in vivo. Our findings indicated the formation of gradient of cell density along the channel axis, with a front edge composed of large leader cells, and compacted followers at the rear. We found that the front and rear zones exhibited p_0 values above the solid to fluid transition ($p_0 = 3.81$), suggesting that both zones adopted a fluid-like behavior, regardless the channel aspect ratio. Interestingly, our findings demonstrated that variations of cell densities between rear and front zones do not affect the jamming state of the tissues, suggesting that cell density is not a key determinant of jamming within epithelial tissues. Our results are in agreement with previous results reported by Simon Garcia and coworkers on human bronchial epithelial cells (HBEC; Garcia et al., 2015), suggesting that the jamming transition is mainly driven by changes in cell-cell adhesion and friction. Altogether, our observations point to an ageing process of the epithelial tissue rather than a simple modification of cell density.

By performing time-lapse experiments on young (Day 1) and aged (Day 6) tissues, we demonstrated that the wider the slit-like microchannel, the larger the migrating velocity for young tissues. Interestingly, the migrating velocity of aged tissues (Day 6) exhibited velocities three times slower than young tissues. Our observations support therefore an ageing process leading to a higher fluidization of the front edge and slower migrating velocities, whereas the widening of slit-like microchannels allows to increase the migrating velocity of epithelial tissues. Altogether, our results suggest that ageing of epithelial tissues may induce changes in cell-cell adhesion and friction, whereas confined microenvironments lead to lower migration velocities.

Finally, we investigated whether slit-like geometries can lead to the activation of YAP proteins, which are involved in mechanosensing (Dupont et al., 2011; Park et al., 2019) and in the control of cell-cell and cell-substrate interactions (Calvo et al., 2013; Mohammed, Versaevel, et al., 2019). Our findings indicate that the cytoplasmic to nuclear YAP ratio decreases gradually from the rear to the front, as observed for the cellular density, and that YAP is accumulated and activated in the nucleus of leader cells. Based on the differences reported between leaders and follower cells, it would be therefore very interesting to dissect the role of Rho-associated kinase, that mediates the cytoskeletal tension, and FA kinase (FAK), that regulates adhesion remodeling, to identify the differences of YAP expression in epithelia.

Although further study will be necessary to clarify how YAP activation can be modulated in confined epithelial tissues, these data contribute to the emerging evidence that a 3D spatial confinement modulates the growth of epithelial tissues and validate slit-like microchannels for studying in vitro epithelial tissues in 3D-confined microenvironments, which are reminiscent of pathological scenarios.

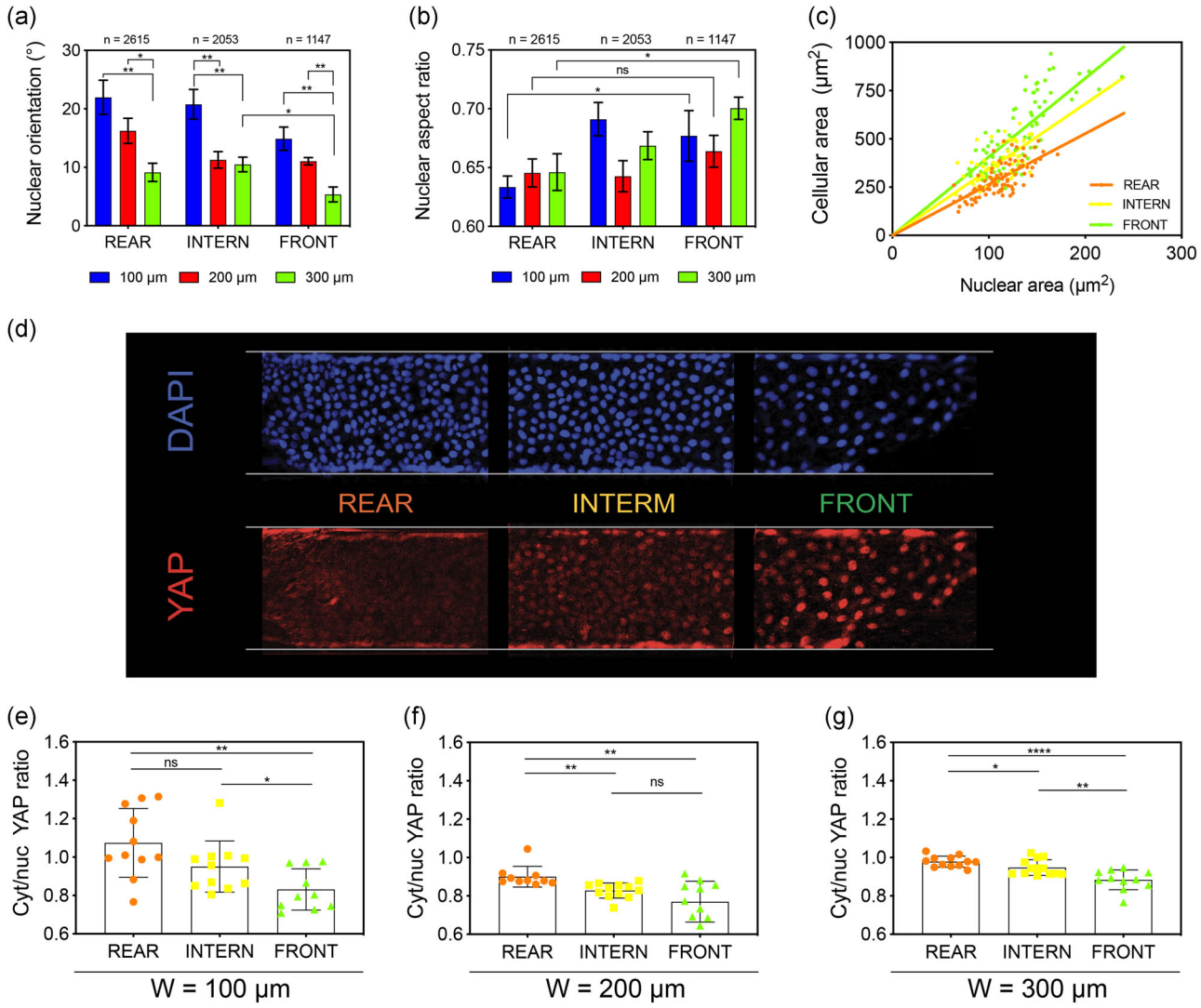

FIGURE 5 (a) Orientation and (b) aspect ratio of the nuclei in the rear, interm, and front zones of epithelial tissues grown in 100 µm (blue), 200 µm (red), and 300 µm (green) wide slit-like microchannels. (c) The cellular area fits linearly with the nuclear area in the three zones. (d) Typical fluorescent images of an epithelial tissues grown in a 200-µm-wide microchannel and immunostained for YAPYes-associated protein (YAP; in red). Nuclei were immunostained in blue with 4',6-diamidino-2-phenylindole (DAPI) to determine the contour of each nucleus. Evolution of the cytoplasmic to nuclear YAP ratio in the rear, interm, and front zones of (e) 100-µm, (f) 200-µm, and (g) 300-µm-wide microchannels. Mean ± *SD*. $11 \leq n \leq 31$ for each condition. $^{*}p < .05$, $^{**}p < .01$, $^{****}p < .0001$ and n.s. not significant [Color figure can be viewed at wileyonlinelibrary.com]

ACKNOWLEDGMENTS

The authors gratefully acknowledge financial support from the Belgian National Fund for Scientific Research (F.R.S.-FNRS, Crédit de Recherches - J009916F) and the FEDER Prostem research project no. 1510614 (Wallonia DG06). L. A., M. L., D. M., C. B., E. V. are financially supported by FRIA (F.R.S.-FNRS).

CONFLICT OF INTERESTS

The authors declare that there are no conflict of interests.

ORCID

Sylvain Gabriele http://orcid.org/0000-0001-8696-8052

REFERENCES

Angelini, T. E., Hannezo, E., Trepat, X., Marquez, M., Fredberg, J. J., & Weitz, D. A. (2011). Glass-like dynamics of collective cell migration. *Proceedings of the National Academy of Sciences*, *108*(12), 4714–4719. https://doi.org/10.1073/pnas.1010059108

Bi, D., Lopez, J. H., Schwarz, J. M., & Manning, M. L. (2015). A density-independent rigidity transition in biological tissues. *Nature Physics*, *11*(12), 1074–1079. https://doi.org/10.1038/nphys3471

Bishop, J. A., Yonescu, R., Batista, D., Begum, S., Eisele, D. W., & Westra, W. H. (2013). Utility of mammaglobin immunohistochemistry as a proxy marker for the ETV6-NTRK3 translocation in the diagnosis of salivary mammary analogue secretory carcinoma. *Human Pathology*, *44*(10), 1982–1988. https://doi.org/10.1016/j.humpath.2013.03.017

Bruyère, C., Versaevel, M., Mohammed, M., Alaimo, A., Luciano, M., Vercruysse, E., & Gabriele, S. (2019). Actomyosin contractility scales with myoblast elongation and enhances differentiation through YAP nuclear export. *Scientific Reports*, *9*, 15565. https://doi.org/10.1038/s41598-019-52129-1

Calvo, F., Ege, N., Grande-Garcia, A., Hooper, S., Jenkins, R. P., Chaudhry, S. I., … Sahai, E. (2013). Mechanotransduction and YAP-dependent matrix remodelling is required for the generation and maintenance of cancer-associated fibroblasts. *Nature Cell Biology*, *15*(6), 637–646. https://doi.org/10.1038/ncb2756

Carpino, G., Renzi, A., Cardinale, V., Franchitto, A., Onori, P., Overi, D., … Gaudio, E. (2016). Progenitor cell niches in the human pancreatic duct system and associated pancreatic duct glands: An anatomical and immunophenotyping study. *Journal of Anatomy*, *228*(3), 474–486. https://doi.org/10.1111/joa.12418

Collins, T. J. (2007). ImageJ for microscopy. *Biotechniques*, *43*(1S), S25–S30. https://doi.org/10.2144/000112517

Coppée, S., Gabriele, S., Jonas, A. M., Jestin, J., & Damman, P. (2011). Influence of chain interdiffusion between immiscible polymers on dewetting dynamics. *Soft Matter*, *7*(21), 9951. https://doi.org/10.1039/c1sm05486d

Dupont, S., Morsut, L., Aragona, M., Enzo, E., Giulitti, S., Cordenonsi, M., … Piccolo, S. (2011). Role of YAP/TAZ in mechanotransduction. *Nature*, *474*(7350), 179–183. https://doi.org/10.1038/nature10137

Farhadifar, R., Röper, J.-C., Aigouy, B., Eaton, S., & Jülicher, F. (2007). The influence of cell mechanics, cell-cell interactions, and proliferation on epithelial packing. *Current Biology*, *17*(24), 2095–2104. https://doi.org/10.1016/j.cub.2007.11.049

Furukawa, K. T., Yamashita, K., Sakurai, N., & Ohno, S. (2017). The epithelial circumferential actin belt regulates YAP/TAZ through nucleocytoplasmic shuttling of merlin. *Cell Reports*, *20*(6), 1435–1447. https://doi.org/10.1016/j.celrep.2017.07.032

Garcia, S., Hannezo, E., Elgeti, J., Joanny, J.-F., Silberzan, P., & Gov, N. S. (2015). Physics of active jamming during collective cellular motion in a monolayer. *Proceedings of the National Academy of Sciences*, *112*(50), 15314–15319. https://doi.org/10.1073/pnas.1510973112

Gittes, G. K. (2009). Developmental biology of the pancreas: A comprehensive review. *Developmental Biology*, *326*(1), 4–35. https://doi.org/10.1016/j.ydbio.2008.10.024

Hoijman, E., Rubbini, D., Colombelli, J., & Alsina, B. (2015). Mitotic cell rounding and epithelial thinning regulate lumen growth and shape. *Nature Communications*, *6*(1), 7355. https://doi.org/10.1038/ncomms8355

Huebner, R. J., & Ewald, A. J. (2014). Cellular foundations of mammary tubulogenesis. *Seminars in Cell & Developmental Biology*, *31*, 124–131. https://doi.org/10.1016/j.semcdb.2014.04.019

Janevska, V., Vanja, F., Saso, B., Vlado, J., Alen, J., Rubens, J., … Blagica, D. (2011). Synovial sarcoma of the liver—A case report. *Macedonian Journal of Medical Sciences*, *4*(2), 185–191. https://doi.org/10.3889/MJMS.1857-5773.2011.0168

Kim, S., & Hilgenfeldt, S. (2015). Cell shapes and patterns as quantitative indicators of tissue stress in the plant epidermis. *Soft Matter*, *11*(37), 7270–7275. https://doi.org/10.1039/C5SM01563D

Loureiro, J., & Oliva, E. (2014). The spectrum of cervical glandular neoplasia and issues in differential diagnosis. *Archives of Pathology & Laboratory Medicine*, *138*(4), 453–483. https://doi.org/10.5858/arpa.2012-0493-RA

Lubarsky, B., & Krasnow, M. A. (2003). Tube morphogenesis. *Cell*, *112*(1), 19–28. https://doi.org/10.1016/S0092-8674(02)01283-7

Maniar, K., & Wei, J. (2017). Pathology of cervical carcinoma. *The Global Library of Women's Medicine*, https://doi.org/10.3843/GLOWM.10230

Martín-Belmonte, F., Yu, W., Rodríguez-Fraticelli, A. E., Ewald, A., Werb, Z., Alonso, M. A., & Mostov, K. (2008). Cell-polarity dynamics controls the mechanism of lumen formation in epithelial morphogenesis. *Current Biology*, *18*(7), 507–513. https://doi.org/10.1016/j.cub.2008.02.076

Mohammed, D., Charras, G., Vercruysse, E., Versaevel, M., Lantoine, J., Alaimo, L., … Gabriele, S. (2019). Substrate area confinement is a key determinant of cell velocity in collective migration. *Nature Physics*, *15*, 858–866. https://doi.org/10.1038/s41567-019-0543-3

Mohammed, D., Versaevel, M., Bruyère, C., Alaimo, L., Luciano, M., Vercruysse, E., … Gabriele, S. (2019). Innovative tools for mechanobiology: Unraveling outside-in and inside-out mechanotransduction. *Frontiers in Bioengineering and Biotechnology*, *7*, 162. https://doi.org/10.3389/fbioe.2019.00162

Neto, F., Klaus-Bergmann, A., Ong, Y. T., Alt, S., Vion, A.-C., Szymborska, A., … Gerhardt, H. (2018). YAP and TAZ regulate adherens junction dynamics and endothelial cell distribution during vascular development. *eLife*, *7*, e31037. https://doi.org/10.7554/eLife.31037

Park, J., Kim, D.-H., Shah, S. R., Kim, H.-N., Kshitiz, Kim, P., … Levchenko, A. (2019). Switch-like enhancement of epithelial–mesenchymal transition by YAP through feedback regulation of WT1 and Rho-family GTPases. *Nature Communications*, *10*(1), 2797. https://doi.org/10.1038/s41467-019-10729-5

dePaula, F., Teshima, T. H. N., Hsieh, R., Souza, M. M., Nico, M. M. S., & Lourenco, S. V. (2017). Overview of human salivary glands: Highlights of morphology and developing processes: Overview of human salivary gland development. *The Anatomical Record*, *300*(7), 1180–1188. https://doi.org/10.1002/ar.23569

Poujade, M., Grasland-Mongrain, E., Hertzog, A., Jouanneau, J., Chavrier, P., Ladoux, B., … Silberzan, P. (2007). Collective migration of an epithelial monolayer in response to a model wound. *Proceedings of the National Academy of Sciences*, *104*(41), 15988–15993. https://doi.org/10.1073/pnas.0705062104

Reichert, M., & Rustgi, A. K. (2011). Pancreatic ductal cells in development, regeneration, and neoplasia. *Journal of Clinical Investigation*, *121*(12), 4572–4578. https://doi.org/10.1172/JCI57131

Riaz, M., Versaevel, M., Mohammed, D., Glinel, K., & Gabriele, S. (2016). Persistence of fan-shaped keratocytes is a matrix-rigidity-dependent mechanism that requires α5β1 integrin engagement. *Scientific Reports*, *6*(1), 34141. https://doi.org/10.1038/srep34141

Szabó, B., Szöllösi, G. J., Gönci, B., Jurányi, Zs, Selmeczi, D., & Vicsek, T. (2006). Phase transition in the collective migration of tissue cells: Experiment and model. *Physical Review E*, *74*(6), 061908. https://doi.org/10.1103/PhysRevE.74.061908

Tlili, S., Gauquelin, E., Li, B., Cardoso, O., Ladoux, B., Delanoë-Ayari, H., & Graner, F. (2018). Collective cell migration without proliferation: Density determines cell velocity and wave velocity. *Royal Society Open Science*, *5*(5), 172421. https://doi.org/10.1098/rsos.172421

Trepat, X., Wasserman, M. R., Angelini, T. E., Millet, E., Weitz, D. A., Butler, J. P., & Fredberg, J. J. (2009). Physical forces during collective cell migration. *Nature Physics*, *5*(6), 426–430. https://doi.org/10.1038/nphys1269

Vedula, S. R. K., Leong, M. C., Lai, T. L., Hersen, P., Kabla, A. J., Lim, C. T., & Ladoux, B. (2012). Emerging modes of collective cell migration induced by geometrical constraints. *Proceedings of the National Academy of Sciences*, *109*(32), 12974–12979. https://doi.org/10.1073/pnas.1119313109

Versaevel, M., Grevesse, T., & Gabriele, S. (2012). Spatial coordination between cell and nuclear shape within micropatterned endothelial cells. *Nature Communications*, *3*(1), 671. https://doi.org/10.1038/ncomms1668

Versaevel, M., Grevesse, T., Riaz, M., Lantoine, J., & Gabriele, S. (2014). Micropatterning hydroxy-PAAm hydrogels and sylgard 184 silicone elastomers with tunable elastic moduli. *Methods in Cell Biology*, *121*, 33–48. https://doi.org/10.1016/B978-0-12-800281-0.00003-8, https://www.sciencedirect.com/science/article/pii/B9780128002810000038?via%3Dihub

Versaevel, M., Riaz, M., Grevesse, T., & Gabriele, S. (2013). Cell confinement: Putting the squeeze on the nucleus. *Soft Matter*, *9*(29), 6665–6676. https://doi.org/10.1039/C3SM00147D

Vicsek, T., & Zafeiris, A. (2012). Collective motion. *Physics Reports*, *517*(3–4), 71–140. https://doi.org/10.1016/j.physrep.2012.03.004

Williams, J. M., & Daniel, C. W. (1983). Mammary ductal elongation: Differentiation of myoepithelium and basal lamina during branching morphogenesis. *Developmental Biology*, *97*(2), 274–290. https://doi.org/10.1016/0012-1606(83)90086-6

Xi, W., Sonam, S., Beng Saw, T., Ladoux, B., & Teck Lim, C. (2017). Emergent patterns of collective cell migration under tubular confinement. *Nature Communications*, *8*(1), 1517. https://doi.org/10.1038/s41467-017-01390-x

Yao, S. F. (2009). Pathology of cervical carcinoma. *The Global Library of Women's Medicine*, https://doi.org/10.3843/GLOWM.10230

Yevick, H. G., Duclos, G., Bonnet, I., & Silberzan, P. (2015). Architecture and migration of an epithelium on a cylindrical wire. *Proceedings of the National Academy of Sciences*, *112*(19), 5944–5949. https://doi.org/10.1073/pnas.1418857112

SUPPORTING INFORMATION

Additional supporting information may be found online in the Supporting Information section.

How to cite this article: Alaimo L, Luciano M, Mohammed D, et al. Engineering slit-like channels for studying the growth of epithelial tissues in 3D-confined spaces. *Biotechnology and Bioengineering*. 2020;1–10. https://doi.org/10.1002/bit.27446